Available online at www.sciencedirect.com
ScienceDirect
International Journal of Multiphase Flow 33 (2007) 1255–1270
International Journal of Multiphase Flow
www.elsevier.com/locate/ijmulflow

Modeling the evolution of droplet size distribution in two-phase flows

László E. Kollár *, Masoud Farzaneh

NSERC/Hydro-Québec/UQAC Industrial Chair on Atmospheric Icing of Power Network Equipment (CIGELE) and Canada Research Chair on Atmospheric Icing Engineering of Power Networks (INGIVRE) at the University of Québec at Chicoutimi, 555 Boulevard de l'Université, Chicoutimi, Québec, Canada G7H 2B1

Received 28 November 2006; received in revised form 26 March 2007

Abstract

A theoretical model is developed in the present study to simulate droplet motion and the evolution of droplet size distribution (DSD) in two-phase air/dispersed water spray flows. The model takes into account several processes which influence DSD and droplet trajectory: droplet collision and coalescence, evaporation and cooling, gravitational settling, and turbulent dispersion of dispersed phase. The DSDs determined by the model at different locations in a two-phase flow are evaluated by comparing them to experimental observations obtained in an icing wind tunnel. The satisfactory coincidence between simulation and experimental results proves that the model is reliable when modeling two-phase flows under icing conditions. The model is applied for two particular examples in which the modification of DSD is calculated in two-phase flows under conditions describing in-cloud icing and freezing drizzle.

Keywords: Droplet collision; Droplet size distribution; Evaporation; Turbulent dispersion; Two-phase flow

1. Introduction

One of the most important factors influencing atmospheric icing processes is the droplet size distribution (DSD) of the aerosol cloud. A typical way to model atmospheric icing and the modification of the droplet cloud preceding ice formation is to produce an air/dispersed water two-phase flow in an icing wind tunnel, and exposing an icing object to this flow. The aerosol cloud undergoes significant changes before reaching the icing object; and the DSD of the dispersed phase appears to be an important characteristic which is modified, among others. Several factors are responsible for this modification, including interactions between the dispersed and carrying phases resulting in evaporation, mutual interactions within the dispersed phase known as binary droplet collisions, and the effect of external forces leading to gravitational settling of droplets and

* Corresponding author. Tel.: +1 418 545 5011/5606; fax: +1 418 545 5012.
E-mail address: laszlo_kollar@uqac.ca (L.E. Kollár).
URL: http://www.cigele.ca

0301-9322/$ - see front matter © 2007 Elsevier Ltd. All rights reserved.
doi:10.1016/j.ijmultiphaseflow.2007.04.002

vertical variation of the DSD. The extent to which these processes affect the characteristics of the aerosol cloud depends on the level of turbulence in the air flow. The turbulence also plays a key-role in the formation of aerosol clouds in wind-tunnel experiments. High levels of turbulence cause unrealistic thermodynamic processes in the tunnel and unnatural ice accretion. A certain level of turbulence, however, is essential to assure mixing and homogeneity in the cloud.

Models of two-phase flows have been presented in a vast number of publications. Crowe et al. (1977) developed a computational model which solved gas flow equations and droplet equations, and also considered the decrease of droplet mass and temperature due to evaporation and cooling; they ignored, however, the effects of turbulence on droplet dispersion and collisions between droplets. Dukowicz (1980) proposed a stochastic approach to consider turbulence dispersion of droplets, which was elaborated for thick sprays by O'Rourke and Bracco (1980), and modified in Gosman and Ioannides (1981) and in Marek and Olsen (1986). O'Rourke and Bracco (1980) also considered droplet collisions and coalescence in their model by a stochastic approach, which was subsequently applied in Gavaises et al. (1996). The different outcomes of binary droplet collisions were included in the composite collision outcome model of Post and Abraham (2002). The developments of Ko and Ryou (2005) took into account the formation of satellite droplets, which are the results of high-kinetic-energy collisions between droplets (Orme, 1997). The relative velocity of colliding droplets is usually low in flows modeling atmospheric icing processes; therefore the formation of satellite droplets was neglected in a preceding study by the present authors (Kollár et al., 2005a), and the composite collision outcome model was improved in the range of low relative velocities of colliding droplets. An improved model (Kollár et al., 2005b) includes the effects of both the droplet collision and the evaporation and cooling; it ignores, however, the turbulent dispersion of droplets. The importance of this latter process was already emphasized by Kollár et al. (2005a), who predicted that the main reason for the discrepancy between their theoretical and experimental results was the consequence of neglecting turbulence droplet dispersion. The present developments overcome this deficiency of the previous model.

The main goal of this paper is to construct an improved model of two-phase flows, which applies our previously developed model for droplet collisions, calculates the modifications in droplet mass and temperature due to evaporation and cooling, takes into account the effects of turbulence on droplet dispersion, and thus, is capable of simulating the evolution of DSD in the flow. This model also considers the deflection of droplet trajectories due to gravity, and thereby, it is applicable to determine the vertical separation of droplets of different sizes in a horizontal flow. A further achievement of this research is the validation of the results provided by the model by means of DSD measurements in the test section of a wind tunnel. Finally, the model is applied to simulate the evolution of DSD and the vertical separation of droplets under in-cloud icing and freezing drizzle conditions as modeled in an icing wind tunnel.

2. Processes influencing DSD

This section discusses four processes which have great influence on droplet size and trajectory, and whose effects are considered in the model: (i) droplet collision and coalescence, (ii) evaporation and cooling, (iii) gravitational settling, and (iv) turbulent dispersion of droplets.

2.1. Droplet collision and coalescence

The binary droplet collision phenomenon is discussed in detail and a composite collision outcome model is constructed in Kollár et al. (2005a); a brief summary follows. When two droplets interact during flight, five distinct regimes of outcomes may be distinguished: (i) coalescence after minor deformation (or slow coalescence), (ii) bouncing, (iii) coalescence after substantial deformation, (iv) reflexive separation, and (v) stretching separation. The phenomenon of droplet collision is controlled by several physical parameters, but the outcome of collisions is usually described by three non-dimensional parameters: (i) Weber number, We, which is the ratio of the inertial force to the surface force, (ii) impact parameter, B, which is the distance from the center of one droplet to the relative velocity vector placed on the center of the other droplet, divided by the sum of radii of colliding droplets, and (iii) droplet size ratio, Δ, which is the ratio of diameter of the smaller droplet to that of the larger one. Boundary curves between the regions of possible outcomes are proposed in terms of

these parameters. Criteria for stretching separation, reflexive separation and bounce are derived in Brazier-Smith et al. (1972), Ashgriz and Poo (1990), Estrade et al. (1999), respectively. The model of Kollár et al. (2005a) applies these transition curves, while the condition of slow coalescence is based on the experimental results reported in Qian and Law (1997). The stretching separation criterion is based on energy consideration, and is written as follows:

$$We > \frac{4.8}{B^2}\frac{\lfloor 1+\gamma^2-(1+\gamma^3)^{2/3}\rfloor(1+\gamma^3)^{11/3}}{\gamma^6(1+\gamma)^2}, \tag{1}$$

where $\gamma = 1/\Delta$. Curve A in Fig. 1 represents this condition on the B–We plane for a specific value of Δ. The condition of reflexive separation is that the reflexive kinetic energy exceed 75% of the nominal surface energy, which can be expressed as follows:

$$We > 3[7(1+\Delta^3)^{2/3}-4(1+\Delta^2)]\frac{\Delta(1+\Delta^3)^2}{\Delta^6\eta_1+\eta_2}, \tag{2}$$

where

$$\eta_1 = 2(1-\xi)^2(1-\xi^2)^{1/2}-1, \quad \eta_2 = 2(\Delta-\xi)^2(\Delta^2-\xi^2)^{1/2}-\Delta^3 \quad \text{and} \quad \xi = \frac{1}{2}B(1+\Delta).$$

This condition defines the transition curve B in Fig. 1. The criterion for bouncing assumes that the initial kinetic energy of the droplet does not exceed the energy required to produce a limit deformation. Otherwise, colliding droplets are coalesced, which condition takes the form:

$$We > \frac{\Delta(1+\Delta^2)(4\phi'-12)}{\chi(1-B^2)}, \tag{3}$$

where

$$\chi = \begin{cases} 1-(2-\kappa)^2(1+\kappa)/4 & \text{if } \kappa > 1.0 \\ \kappa^2(3-\kappa)/4 & \text{if } \kappa \leqslant 1.0 \end{cases}, \quad \kappa = (1-B)(1+\Delta)$$

and ϕ' is the shape factor with a proposed value of 3.351. The corresponding curve in Fig. 1 is indicated by C. The boundary curve between slow coalescence and bounce is the line joining two given points (curve D in Fig. 1). One of these points separates the regime of bounce from that of coalescence after substantial deformation for head-on collisions, while the other point is the one where the Weber number is zero and the impact parameter is unity. This collision model is applicable to determine the outcome of collision as well as the size, velocity and temperature of post-collision droplet or droplets, according to the conservation of mass, momentum and energy, respectively.

Simulation results presented in Kollár et al. (2005a) showed how droplet collision and coalescence affected droplet size. The number of small droplets decreases and that of large droplets increases so that the median

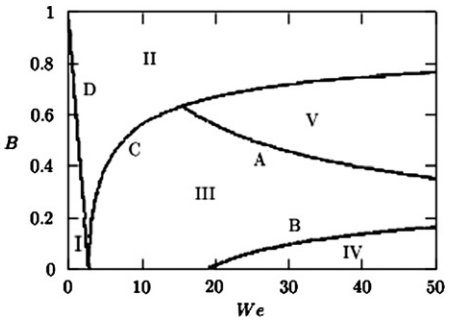

Fig. 1. Collision outcomes on the B–We plane for $\Delta = 1$; I: coalescence after minor deformation (or slow coalescence); II: bouncing; III: coalescence after substantial deformation; IV: reflexive separation; V: stretching separation.

volume diameter (MVD) may be modified significantly depending on ambient conditions. The number of middle-size droplets with diameters close to the MVD does not change significantly, because the number of droplets of diameters in this range that coalesce and form larger droplets, as well as the number of coalescences that result in droplets of diameters in this range, are approximately the same.

2.2. Evaporation and cooling

A method to calculate the decrease of droplet mass and temperature due to evaporation and cooling is based on Beard and Pruppacher (1971), Pruppacher and Klett (1978). This section recalls the formulae, but the reader is advised to see the above references for details. The rate of droplet mass, Δm, which is evaporated during the time interval, Δt, is obtained as follows:

$$\frac{\Delta m}{\Delta t} = -\frac{\pi d D_{\mathrm{f}}(e_{\mathrm{w}}(T_{\mathrm{d}}) - RH_{\mathrm{a}} e_{\mathrm{w}}(T_{\mathrm{a}}))}{R_{\mathrm{w}} T_{\mathrm{f}}\left(1 - \frac{e_{\mathrm{f}}}{p_{\mathrm{st}}}\right)} Sh, \tag{4}$$

where d is the droplet diameter, $e_{\mathrm{w}}(T_{\mathrm{d}})$ and $e_{\mathrm{w}}(T_{\mathrm{a}})$, the pressures of saturated water vapor at droplet temperature, T_{d}, and air temperature, T_{a}, respectively, RH_{a}, the relative humidity of air, Sh, the Sherwood number, R_{w}, the gas constant for water vapor, p_{st}, the static pressure of air, and the subscript f refers to film formation on the evaporation surface involving droplet temperature and air temperature, and the corresponding quantities $T_{\mathrm{f}} = (T_{\mathrm{d}} + T_{\mathrm{a}})/2$, $e_{\mathrm{f}} = (e_{\mathrm{w}}(T_{\mathrm{d}}) + e_{\mathrm{w}}(T_{\mathrm{a}}))/2$ and $D_{\mathrm{f}} = D_{\mathrm{w}}(T_{\mathrm{f}})$ are, respectively, the mean values over the transfer path of the temperature, pressure of saturated water vapor and diffusivity of water vapor, D_{w}. The Sherwood number is defined by the Reynolds number based on air velocity, Re_{a}, and the Schmidt number, Sc, as follows:

$$Sh = 2(0.78 + 0.308 Re_{\mathrm{a}}^{0.5} Sc^{0.33}). \tag{5}$$

The change in droplet temperature, ΔT_{d}, during the time interval, Δt, is obtained from the heat balance:

$$c_{\mathrm{w}} m \frac{\Delta T_{\mathrm{d}}}{\Delta t} = \alpha d^2 \pi (T_{\mathrm{a}} - T_{\mathrm{d}}) + L_{\mathrm{ev}} \frac{\Delta m}{\Delta t}, \tag{6}$$

where m is the droplet mass, c_{w}, the specific heat of water, L_{ev}, the latent heat of vaporization of water, and the heat transfer coefficient, α, is determined by the following expression:

$$\alpha = \frac{Nu \lambda_{\mathrm{a}}}{d}, \tag{7}$$

where λ_{a} is thermal conductivity of air at the temperature of droplet surface, and the Nusselt number, Nu, is defined by Whitaker (1972):

$$Nu = 2 + \left(0.4 Re_{\mathrm{a}}^{0.5} + 0.06 Re_{\mathrm{a}}^{0.67}\right) Pr^{0.4} \left(\frac{\mu_{\mathrm{a}}(T_{\mathrm{a}})}{\mu_{\mathrm{a}}(T_{\mathrm{d}})}\right)^{0.25}. \tag{8}$$

The Pr denotes Prandtl number, while $\mu_{\mathrm{a}}(T_{\mathrm{a}})$ and $\mu_{\mathrm{a}}(T_{\mathrm{d}})$ are dynamic viscosity of air at air temperature and droplet temperature, respectively. The T_{d} is droplet temperature at the beginning of the time step, and $\Delta m/\Delta t$ is obtained from Eq. (4).

Simulation results presented in Kollár et al. (2005b) showed that the effects of evaporation and cooling were negligible for low air temperatures and for values of relative humidity of air close to unity; they became significant, however, as air temperature approached or exceeded 0 °C and the relative humidity of air dropped below 0.75.

2.3. Gravitational settling

Gravity is usually not considered in aircraft icing models due to the high air velocity and the corresponding dominance of drag forces; it significantly affects, however, droplet trajectory in low-speed wind tunnels and in atmospheric icing processes with gentle winds. The effect of gravity was examined in Kollár et al. (2005a), and

this study revealed that gravity was not negligible for low air velocities (5–10 m/s); moreover, the influence of gravity on droplet motion was amplified for large droplets. The vertical deflection of droplet trajectories as well as the vertical component of droplet velocities decreased with air velocity and increased with droplet size. Consequently, gravity causes separation of droplets of different sizes, which leads to vertical variation in DSD and liquid water content. A term considering gravity is included in the droplet equation which will be presented in Section 3.

2.4. Turbulent dispersion of droplets

The effect of turbulence on droplet motion is considered by a stochastic approach which was introduced by Dukowicz (1980). The instantaneous gas velocity, $\mathbf{u}$, is determined by adding a fluctuating component, $\mathbf{u}'$, to the gas velocity, $\bar{\mathbf{u}}$, in the droplet equation. The fluctuating component, $\mathbf{u}'$, is chosen from a Gaussian probability distribution with a standard deviation of $(2k/3)^{0.5}$, where k denotes turbulent kinetic energy. The value of the fluctuating component is changed at the beginning of each droplet–turbulent eddy interaction. The time interval of this interaction is the minimum of the eddy lifetime, t_e, and the transit time, t_r, over which the droplet traverses the eddy (Gosman and Ioannides, 1981). The eddy lifetime is obtained from

$$t_e = \frac{l_e}{|\mathbf{u}'|}. \tag{9}$$

The l_e is the characteristic size of the turbulent eddy given by

$$l_e = \frac{C_\mu^{0.75} k^{1.5}}{\varepsilon}, \tag{10}$$

where $C_\mu = 0.09$, and ε is turbulent dissipation. The estimation for transit time takes the form:

$$t_r = -\tau \ln\left(1 - \frac{l_e}{\tau|\mathbf{u} - \mathbf{v}|}\right), \tag{11}$$

where $\tau = 4\rho_d d/(3\rho_a C_D|\mathbf{u} - \mathbf{v}|)$, ρ_d and ρ_a are the droplet and air densities, respectively, C_D, the drag coefficient, and $\mathbf{v}$, the droplet velocity. When $l_e/(\tau|\mathbf{u} - \mathbf{v}|) > 1$, Eq. (11) does not have a solution, therefore it is assumed that the time of droplet–eddy interaction is equal to the eddy lifetime, t_e.

3. Model description

A two-dimensional model of two-phase air/dispersed water flows will be constructed in this section. The air velocity field together with turbulent parameters are determined first. These data serve as input for the model which solves the droplet equation, tracks droplet trajectories, and calculates droplet parameters such as size, velocity and temperature, which are modified by the processes described in Section 2. Thus, this model considers the influence of the carrier phase on particle motion, but it assumes that the dispersed phase does not change the continuous fluid phase. Thick spray droplets, however, may affect the gas velocity, and may modify the turbulence intensity of the carrier phase. Consequently, some models exist, which take into account two-way coupling between the phases (e.g. Crowe et al., 1977; Edson et al., 1996; Valentine and Decker, 1995). Numerous criteria have been proposed to establish whether the two-way exchange of mass, momentum and thermal energy between the phases is negligible or significant. Only a few of them will be listed here, which were examined in the present study to confirm that the one-way coupled model is an acceptable simplification in the cases investigated. Gore and Crowe (1989) obtained that if the ratio of particle diameter to turbulent length scale, d/l_e, was less than 0.1, then particles did not increase turbulent intensity. Hetsroni (1989) used the Reynolds number, Re, based on the gas-droplet relative velocity (see Section 3.2) to define a condition. He reported that the dispersed phase did not enhance turbulence in the gas phase, if $Re \leqslant 110$. Although the presence of particles for which the ratio d/l_e or the Reynolds number Re are less than their critical values may suppress turbulence in the gas phase, the decrease of turbulence intensity in this case is much smaller than its increase when $d/l_e > 0.1$ or $Re > 110$. Both of these conditions for neglecting turbulence enhancement are satisfied in the cases modeled in this study. Even the largest droplets are two orders of magnitudes smaller than

the turbulent length scale. Although close to the spray-bar in the settling chamber where the relative velocity is higher (10–20 m/s), the Reynolds number, *Re*, may approach its critical value for the highest droplets (with diameter in the range of 100 μm), the average value of Reynolds number is orders of magnitude smaller than the critical value. Gates et al. (1988) examined if the air stream temperature and velocity changed due to heat exchange between the phases. The authors did not formulate any criterion; they assumed, however, that these changes were negligible when the liquid to air mass ratio was less than 1%. Moreover, Wang et al. (2005) reported that the droplets had little effects on air turbulence in typical clouds where the droplet mass loading was on the order of 10^{-3}, which is also the case in the major part of the wind tunnel in our experiments. It should be clear that the liquid to air mass ratio may be significantly higher than 1% in thick sprays as in wind tunnel experiments close to the nozzle; however, the inlet of simulation domain in the present model is defined 50 cm downstream the nozzle outlet where the breakup of liquid jet may be assumed to be completed, and the liquid to air mass ratio already decreases to the range of 1%. Due to the satisfaction of the above conditions, the one-way coupled model was accepted for the cases simulated in this study.

3.1. Air velocity field and turbulent parameters

The air velocity field is determined by the commercial software CFX, which solves the Navier–Stokes equations iteratively by using the finite volume technique. A default tetrahedral element discretization is used for meshing. Boundary conditions assume no slip at the tunnel walls and zero velocity perpendicular to the wall. Velocities at the inlet and outlet and the geometry of the computational domain are defined as input data for this computation. This software is applicable for simulations in three dimensions, but the droplet trajectory code is two dimensional only, therefore results provided in the middle vertical plane by CFX are used in the simulation of droplet motion. This software is also capable of computing turbulent kinetic energy and turbulent dissipation once the user defines what turbulence model should be applied. More realistic turbulence data were obtained, however, when the level of turbulence and the size of turbulent eddy at the inlet and outlet were defined as inputs in the droplet trajectory code, and their variations through the computational domain were approximated by a simple function which may be chosen according to the modeled process. Then, the turbulent kinetic energy, k, may be obtained from the level of turbulence, Tu, as follows:

$$k = \frac{1}{2}\bar{\mathbf{u}}^2 Tu^2 \tag{12}$$

and Eq. (10) yields turbulent dissipation, ε.

3.2. Droplet equation

The droplet trajectory code is based on the particle-source-in-cell model constructed by Crowe et al. (1977) and the droplet equation derived by Maxey and Riley (1983):

$$\frac{\pi}{6}d^3(\rho_\mathrm{d} + 0.5\rho_\mathrm{a})\frac{\mathrm{d}\mathbf{v}}{\mathrm{d}t} = \frac{\pi}{6}d^3(\rho_\mathrm{d} - \rho_\mathrm{a})\mathbf{g} + 3\pi d\mu_\mathrm{a} f(\mathbf{u} - \mathbf{v}) + \frac{\pi}{4}d^3\rho_\mathrm{a}\frac{\mathrm{D}\mathbf{u}}{\mathrm{D}t}, \tag{13}$$

where $\mathbf{g}$ is the gravity vector, f considers Stokes drag, and D stands for total derivative. The last term in Eq. (13) was neglected in Kollár et al. (2005a), because the air velocity was constant. The present model takes into account the acceleration of the flow; however, this term is at least one to two orders of magnitude less than the other ones for all the cases examined, therefore the same droplet equation is used as in Kollár et al. (2005a). The parameter, f, and the drag coefficient, C_D, are defined by the following expressions, respectively (Crowe et al., 1977):

$$f = 1 + 0.15Re^{0.687} \quad \text{and} \quad C_\mathrm{D} = \frac{24}{Re}f, \tag{14}$$

where the Reynolds number, Re, is based on the gas-droplet relative velocity:

$$Re = \frac{\rho_\mathrm{a}|\mathbf{u} - \mathbf{v}|d}{\mu_\mathrm{a}}. \tag{15}$$

Then, assuming that $\rho_d \gg \rho_a$, and defining the following non-dimensional parameters: $\mathbf{U} = \mathbf{u}/u$, $\mathbf{V} = \mathbf{v}/u$ and $T = tu/l$, where $u = |\mathbf{u}|$ and l is the horizontal length of the computational domain, the non-dimensional droplet equation is obtained after some algebraic operations:

$$\frac{d\mathbf{V}}{dT} = \frac{l}{u^2}\mathbf{g} + \frac{18\mu_a l}{\rho_d d^2 u} f(\mathbf{U} - \mathbf{V}). \tag{16}$$

Since f varies with time, Eq. (16) is integrated numerically by using the Euler scheme in a predictor–corrector mode:

$$\mathbf{V}_* = \mathbf{V}_j + \left.\frac{d\mathbf{V}}{dT}\right|_j \Delta T, \tag{17}$$

$$\mathbf{V}_{j+1} = \mathbf{V}_j + \left(\left.\frac{d\mathbf{V}}{dT}\right|_j + \left.\frac{d\mathbf{V}}{dT}\right|_*\right)\frac{\Delta T}{2}, \tag{18}$$

where ΔT is the non-dimensional time interval, the subscripts j and $j+1$ refer to quantities at the beginning and at the end of the time increment, respectively, while the subscript $*$ refers to an intermediate value. After the droplet velocity, $\mathbf{V}_{j+1}$, at the end of the time increment, ΔT, is determined, the corresponding droplet position, $\mathbf{X}_{j+1}$, is obtained by applying the trapezoidal scheme:

$$\mathbf{X}_{j+1} = \mathbf{X}_j + (\mathbf{V}_j + \mathbf{V}_{j+1})\frac{\Delta T}{2}. \tag{19}$$

3.3. Procedure of computation

Input data for the calculation of air velocity field, i.e. air velocities at the inlet and outlet of the simulated domain, are obtained from measurements, and then velocities are computed at many points in between by the commercial software CFX. The airflow field is subdivided into a series of cells, which are regarded as control volumes. An air velocity is associated with each control volume, which velocity was calculated closest to the midpoint of that control volume. Consequently, the size of control volumes was chosen to be 25 mm, which satisfies the conditions that the difference between the velocities of two neighboring control volumes be small (in the range of few percents of the absolute value of velocity or less), and that their size be at least an order of magnitude greater than the size of the largest parcel. The air velocity field obtained is used as input in the model of two-phase flows, which follows the motion of droplets in the control volumes. Since there are too many droplets to examine individually, they are collected into parcels. The method is based on the concept of the discrete parcel approach (O'Rourke and Bracco, 1980). The number of parcels has to be at least in the range of thousands in order to obtain a reliable statistics; however, increasing number of parcels increase computational costs significantly. As a compromise, 3000 parcels were considered in the simulations, each of which included 3000 droplets. In this case, additional parcels of droplets are still injected in the simulation when some parcels already reached the icing object, and the simulation is terminated after sufficient parcels reached the neighborhood of the icing object to form a distribution, i.e. at least 1000. The water flow may also be manipulated in the model by changing time step or the number of time steps between the injections of two parcels. The time step, however, is limited by the time scales of the processes modeled, of which collision was found to be decisive. The time step should be small enough to avoid that two parcels "jump" each other during simulation; nevertheless it should be large enough to avoid collision immediately at the inlet. Accordingly, the time step was 2.5×10^{-5} s and 5×10^{-5} s in modeling in-cloud icing and freezing drizzle, respectively. Each parcel contains the same number of drops of identical size, velocity and temperature. These droplet parameters at the beginning of the computational domain are also required as input data. They may be obtained from measurements or the user can define them in correspondence with the modeled process. In order to introduce a DSD into the model, the droplet spectrum is first discretized, 5-μm wide bins are thereby created, and the diameter of each droplet is replaced by the arithmetic mean of the corresponding bin. The relative frequencies of the appearance of droplets in each bin are then used to obtain the discrete droplet spectrum. An interval of random numbers corresponds to every discrete value of the droplet diameter, as explained in Kollár et al.

(2005a). Then, a random number is generated for each parcel of droplets and the diameter of each droplet in the parcel is the value in the spectrum that corresponds to the interval of which the random number is an element. Although random numbers are generated according to the input DSD, the final distribution of random numbers may be slightly different due to the finite number of random numbers. Therefore, the following correction is applied: The number of parcels containing droplets from each particular bin is determined by the relative frequency of the appearance of droplets in that bin multiplied by the total number of parcels considered in the simulation. If all the parcels containing droplets from a particular bin have already been introduced into the simulation and the same should be chosen again according to the next generated random number, then a parcel of droplets of the closest greater diameter is taken. If all the larger droplets have also been considered, then a parcel with the smallest and still available droplets is introduced. Further inputs are the ambient conditions, which are assumed to be constant over the computational domain, and turbulence data, i.e. the level of turbulence and size of turbulent eddy. The parameters considering ambient conditions and turbulence data may be prescribed according to the conditions prevailing under the modeled process or may be provided by experiments.

The simulation of the two-phase flow proceeds as follows. The parcels are tracked in space and time as if they were single droplets with the size, mass, velocity and temperature of one droplet from that parcel. The fluctuating component of air velocity is modified after each time interval describing the droplet–turbulent eddy interaction. The actual fluctuating velocity is added to the air velocity at the beginning of each time step, and is considered in the droplet equation. Then the position and velocity of droplets are determined by applying Eqs. (17)–(19), and the droplet size is reduced according to the loss of mass and the droplet temperature is modified due to evaporation and cooling. If the lost mass is greater than or equal to the mass of the droplet itself, then the droplet is evaporated and the parcel is withdrawn from further computation. Afterwards, colliding droplets are sought for. From the collisional point of view, the parcel size is considered larger according to the mass of droplets carried in one parcel. If the distance between two parcels is less than the sum of their radii, they will collide. The outcome of collisions and the sizes and velocities of post-collision droplets are determined by utilizing the composite collision outcome model. If coalescence occurs, then the two parcels are replaced by one parcel in which the mass of droplets is equal to the sum of mass of the two colliding droplets. This process is continued in the next time steps until the termination condition of the simulation is satisfied.

4. Experimental setup and measurement technique

Experiments were carried out at the CIGELE atmospheric icing research wind tunnel (CAIRWT). This facility is a closed-loop, low-speed icing wind tunnel with a total length of about 30 m, including a 3-m long test section with a rectangular cross-section 46 cm high and 91 cm wide. The cross-section of the tunnel at the spray bar is also rectangular with a height of 1.14 m and width of 1.7 m. The tunnel becomes circular 1.5 m downstream from the spray bar with a diameter of 1 m. The cross-section contracts further in the next 1.1 m reaching the final rectangular cross-section with the size of the test section. The distance between the spray-bar and the middle of the test section where the icing object is usually placed is 4.4 m. A draft of this part of the wind tunnel as it is presented in CFX can be seen in Fig. 2. This figure also shows the calculated air velocity field in the middle vertical plane when the air speed in the test section is set at 10 m/s. Water is injected into the air stream through three air-assisted nozzles located on a horizontal spray bar with distances of 20 cm between them. The nozzles are manufactured by Spray System Co. and incorporate stainless steel fluid cap 2050 and stainless steel air cap 67147. The pressures and the flow rates of the water line and air line may be adjusted to requirements. These parameters together with the nozzle characteristics have an influence on the liquid jet break-up, and they determine the resulting DSD at the nozzle outlet. This DSD was measured and its dependence on nozzle-dynamic parameters was scrutinized in detail in Kollár et al. (2006). Additional droplet size measurements were performed in the present project, at different heights in the middle of the test section. The former experimental results serve as input for our model, while results of the latter measurements are used to validate the output of the model.

The DSD was measured by applying the collargol slide impact method (Godard, 1960). A special tool, the cylindrical droplet impact sampler, was constructed to collect droplets. This tool is based on the one proposed by Du (1987), and is described in more detail in Kollár et al. (2006). Droplet samples were collected on a small

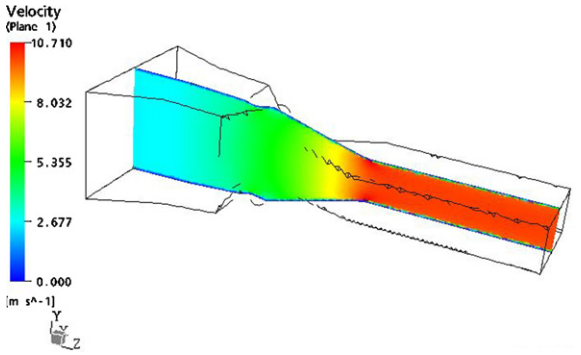

Fig. 2. Part of wind tunnel between spray bar and middle of test section as presented in CFX, including air velocity field in the middle vertical plane for air velocity in test section of 10 m/s.

slide with dimensions of 4.5 cm in length and 2.7 cm in height. Either side of this slide is covered by collargol, which makes it possible to capture droplets and to provide a highly visible droplet pattern. Droplet diameters were measured by using a Scienscope microscope. The input air velocities for CFX calculations were measured by Omega anemometer, while turbulence data at the spray-bar and in the middle of test section were obtained using a TSI hot-wire anemometer IFA300.

5. Simulation of DSD modifications in an icing wind tunnel

The theoretical model explained in detail in Section 3 was implemented by a Fortran computing tool. This model was applied to simulate two-phase flows in an icing wind tunnel where parameters are chosen so as to model natural conditions. In particular, attempts were made to reproduce aerosol clouds formed under in-cloud icing conditions as well as under freezing drizzle conditions. Table 1 summarizes the atmospheric conditions which were assumed during in-cloud icing and during freezing drizzle. The air temperature, however, was always +5 °C during droplet size measurements, because the collargol method is reliable above the freezing point of water (Laforte and Du, 1988). Consequently, the same temperature was chosen in the comparative simulations. The median volume diameters (MVDs) given in the table are the ones obtained at the nozzle outlet for two particular combinations of the nozzle-dynamic parameters, i.e. $p_L = 449$ kPa and $p_A = 483$ kPa for in-cloud icing, and $p_L = 449$ kPa and $p_A = 173$ kPa for freezing drizzle, where p_L and p_A are the pressures in

Table 1
Atmospheric parameters assumed under in-cloud icing and freezing drizzle conditions at the location given in parentheses (air temperature and relative humidity of air are assumed constant)

Atmospheric parameters	In-cloud icing	Freezing drizzle
Air temperature (°C)	−10	−5
Air velocity (m/s) (test section)	20	10
Relative humidity of air (–)	0.95	0.8
Median volume diameter (μm) (settling chamber)	27	62

Table 2
Turbulence data measured at air velocities of 20 m/s (in-cloud icing) and 10 m/s (freezing drizzle) at the location given in parentheses

Turbulence data	$V_a = 20$ m/s (test section)	$V_a = 10$ m/s (test section)
Size of turbulent eddy (cm) (settling chamber)	10.4	11.8
Size of turbulent eddy (cm) (test section)	3.9	4.3
Level of turbulence (%) (settling chamber)	7.8	7.9
Level of turbulence (%) (test section)	0.7	0.6

the water line and in the air line, respectively (see Kollár et al., 2006), and the corresponding measured DSDs are introduced as inputs in the simulations. The initial droplet temperature and droplet velocity were chosen as 20 °C and 20 m/s, respectively, while turbulence data are listed in Table 2. Turbulence data were measured at the spray bar and in the middle of test section, and the decay of turbulence along the tunnel is assumed according to a decreasing power function based on the suggestion of Snyder and Lumley (1971). Further parameters, which were kept constant or were calculated as a function of temperature, are provided in the Appendix.

5.1. Experimental observations

The DSD was measured at four different positions: $y = +7$ cm, 0 cm, -7 cm, and -14 cm, where y denotes vertical distance and $y = 0$ is the mid-height of the test section, which appears at the same level as the spray bar with the nozzles. Table 3 presents the measured MVDs for the two conditions considered. The results show clearly the difference between the sizes of droplets as they occur under in-cloud icing and freezing drizzle conditions, and also the vertical separation of droplets of different sizes due to gravity. Former simulation and experimental results (Kollár et al., 2005a,b) suggested that the effect of gravity was important when the air speed did not exceed 20 m/s. Table 3 confirms this observation. Nearly the same MVDs were measured at different vertical levels for in-cloud icing when the air speed was 20 m/s, although a slight increase towards the bottom of the tunnel may be observed (less than 20% between the utmost and bottommost locations). Furthermore, no value appears at $y = -14$ cm, because the aerosol cloud is not extended until this height, and no droplets were captured here. For freezing drizzle, however, when the air speed was 10 m/s, and droplets were larger, the MVD increased significantly towards the bottom of the tunnel (more than three times greater at the bottom than at the top), and many droplets were captured even at the location $y = -14$ cm.

Fig. 3 compares four DSDs, those at the nozzle outlet and in the mid-height of the test section for both conditions examined. The aerosol cloud modeling freezing drizzle includes larger droplets even initially than the cloud produced under in-cloud icing conditions, which is in accordance with the natural processes. Droplets increase in size in both cases as they reach the test section, which is mainly a consequence of droplet col-

Table 3
MVDs measured at different vertical levels under in-cloud icing and freezing drizzle conditions

Vertical level (cm)	MVD (μm) (in-cloud icing)	MVD (μm) (freezing drizzle)
+7	37	56
0	41	77
−7	44	101
−14	–	182

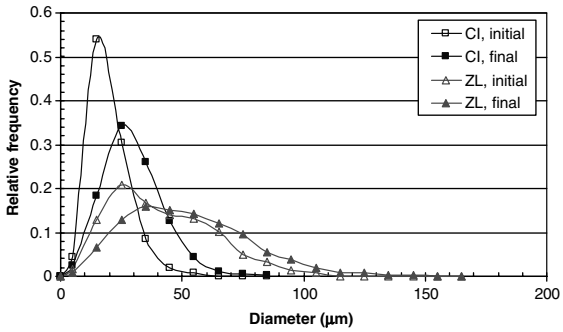

Fig. 3. Measured DSDs under in-cloud icing (CI) and freezing drizzle conditions (ZL) at the nozzle outlet (initial) and in mid-height of the test section (final).

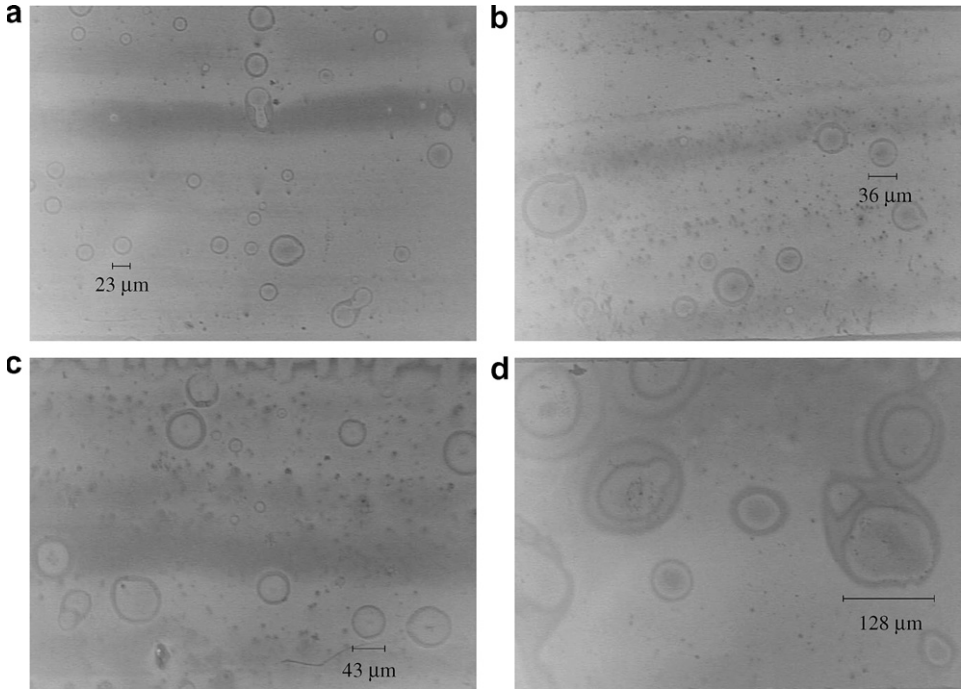

Fig. 4. Slides with captured droplets as seen under a microscope (a) in-cloud icing conditions, $y = +7$ cm, (b) in-cloud icing conditions, $y = -7$ cm, (c) freezing drizzle conditions, $y = +7$ cm and (d) freezing drizzle conditions, $y = -7$ cm. Scale shows diameter of a droplet before impaction.

lision, because two smaller droplets form a larger one when the collision outcome is coalescence. The size of an individual droplet decreases due to evaporation, but the decrease in the size of large droplets is negligible, while the smallest droplets are evaporated completely; therefore, this phenomenon may result in either increasing or decreasing droplet size, depending on cloud characteristics.

Small parts of some of the slides with captured droplets are shown in Fig. 4, as seen under a microscope. Fig. 4a and b show droplets captured under in-cloud icing conditions at $y = +7$ cm and $y = -7$ cm, respectively, while Fig. 4c and d show droplets under freezing drizzle conditions at the same locations. Although only a small fraction of the captured droplets is visible in each figure, they show clearly the difference between droplet sizes under different conditions and at different vertical levels. The tendencies, as can be observed in these pictures, coincide with those discussed in the previous two paragraphs. Fig. 4 also shows some colliding droplets; it should be clear, however, that the diameter of those droplets cannot be measured since their impression is not circular. The diameter of one droplet is indicated in each picture, which may serve as a scale. This scale shows the diameter of the droplet before impaction, which is three times less than the diameter of droplet impression on the slide. Laforte and Du (1988) proposed this comparative factor by which the diameter of impression should be divided in order to obtain the diameter of droplet before impaction.

5.2. Comparison of computed and measured results

Simulation results provide size, position, velocity and temperature of each droplet at the end of the computational domain. The domain where droplets appear in the middle of test section is divided vertically into four and eight intervals when modeling in-cloud icing and freezing drizzle, respectively. The MVDs at each interval are calculated and presented in Fig. 5 together with the measured MVDs. For the sake of comparison, simulations under the same conditions are repeated without considering turbulence within the dispersed phase. Fig. 5 emphasizes the role of turbulence, because simulation results approximate experimental observations

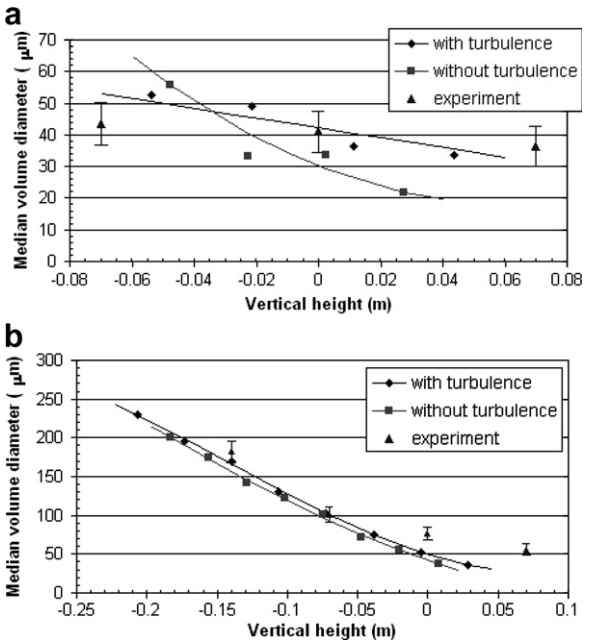

Fig. 5. Computed and measured MVDs at different vertical levels of the test section (a) in-cloud icing conditions and (b) freezing drizzle conditions.

significantly better when turbulence is considered. Kollár et al. (2005a) concluded that the former version of the model, excluding evaporation and turbulence of the dispersed phase, underestimates the dispersion of droplets. The present model provides improved results from two points of view: (i) the vertical domain in the middle of test section where droplets occur is extended, and (ii) the tendency of droplet size to increase towards the bottom of the tunnel approximates nearer the measured ones. Both of these improvements may be owing to the consideration of turbulence dispersion, which causes the extension of droplet cloud and the appearance of a few larger droplets even above the $y = 0$ level. Turbulence also intensifies droplet collision, which fact explains why the MVDs obtained under freezing drizzle conditions and considering turbulence are consistently greater than those obtained with the model ignoring turbulence. As a result, computed and measured results in the bottom half of the tunnel coincide, although the model still underestimates the appearance of droplets in the top half of the tunnel. The improvement, however, as compared to the model of Kollár et al. (2005a), is remarkable; the computed MVD in the upper part of the tunnel falls within the measurement error in the case of in-cloud icing. The measurement error is represented in Fig. 5 by the error bars which correspond to ± 4.5 μm $\pm$ 5% (Kollár et al., 2006).

Fig. 6 shows DSDs at different vertical levels in the test section where droplet size was measured under in-cloud icing and freezing drizzle conditions, and compares them with calculated results. Droplets occurring within 7 cm-wide intervals are considered in the calculations. This is a wide interval as compared to the 2.7-cm-height of the slides where droplets were captured in the experiments, but this wider interval was chosen in order to have enough droplets to form a DSD. The width of this interval was reduced to 3 cm at the level of $y = -14$ cm for freezing drizzle only, because much more droplets appear above this level than below it, and those droplets are smaller; thus, the resulting DSD of the 7 cm-wide interval significantly underestimated the measured one. Nevertheless the number of droplets in a 3 cm-wide interval close to the bottom of the tunnel is low, which fact results in a more fluctuating curve in Fig. 6b. Moreover, DSD is not calculated at the level of $y = +7$ cm for freezing drizzle, because very few droplets were obtained even in a 7 cm-wide interval around this level. This fact results from the underestimation of droplet dispersion in the top half of the tunnel, which is also the reason for the smaller calculated droplets at $y = +7$ cm for in-cloud icing and at $y = 0$ cm for freezing drizzle, as can be seen in Fig. 6. However, the simulation provides satisfactory results in the previous case ($y = +7$ cm for in-cloud icing), i.e. the discrepancy between computed and measured values falls within the

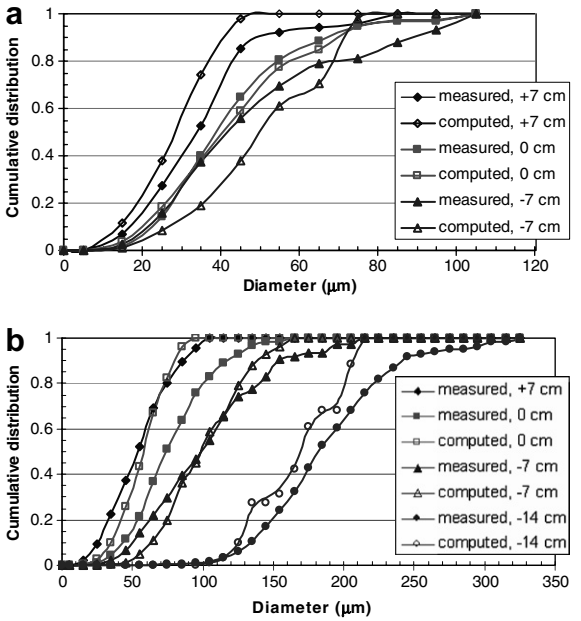

Fig. 6. Computed and measured cumulative distributions at different vertical levels of the test section (a) in-cloud icing conditions and (b) freezing drizzle conditions.

range of measurement error. The same observation can be made for the results obtained at $y = -7$ cm for in-cloud icing and at $y = -14$ cm for freezing drizzle, while excellent coincidence occurs at $y = 0$ cm for in-cloud icing and at $y = -7$ cm for freezing drizzle.

Since a temperature above the freezing point of water was chosen in the calculations above, which condition is not in accordance with natural in-cloud icing and freezing drizzle phenomena, additional simulations were carried out considering freezing temperatures as given in Table 1. This modification has a considerable effect on evaporation only. Droplets lose less mass due to evaporation, which increases the average droplet size; however, some small droplets do not evaporate completely, which decreases the average droplet size; thus, the final result regarding the vertical variation of DSD does not change significantly.

An additional set of simulations were carried out to show the effects of turbulence on droplet dispersion and on droplet size in the test section. In-cloud icing conditions were applied in these simulations as given in Table 1. In particular, three simulations were performed, turbulence was ignored in the first one, a low level of turbulence, i.e. half of the measured values, was assumed in the second one, while the measured level of turbulence was assumed in the last one. Fig. 7 shows the distribution of droplet parcels in the test section at a fixed instance

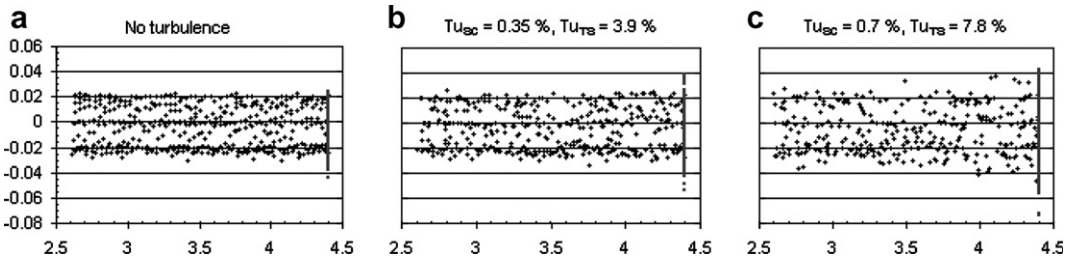

Fig. 7. Position of parcels in the test section at a fixed time (diamonds), and vertical position of parcels which reached the middle of test section before this time (squares), (a) no turbulence is considered, (b) low level of turbulence is assumed, i.e. the level of turbulence at the beginning of settling chamber, Tu_{SC}, and that in the middle of test section, Tu_{TS}, are half of those measured and (c) the measured level of turbulence is assumed; horizontal axis: distance from spray bar, vertical axis: distance form the mid-height of test section.

of time together with the parcels appearing at 4.4 m, which already reached the middle of test section, or, in other words, the end of simulation domain, before this instant of time. It is clearly observable how the disorder of parcel positions increases with the level of turbulence, and how the vertical domain where droplets occur extends when turbulence is considered in the model. The MVDs at the mid-height of test section ($y = 0$ cm) in the three cases are 33 μm, 39 μm and 42 μm. This result is explained by the fact that turbulence enhances droplet collision, which fact results in increasing droplet size due to greater number of coalescences.

6. Conclusions

A theoretical model of two-phase air/dispersed water flows was constructed in the present paper. This model considers several phenomena which affect the size and motion of droplets, namely droplet collision and coalescence, evaporation and cooling, gravitational settling, and turbulent dispersion of dispersed phase. Flows under two particular conditions were simulated by using this model and by wind-tunnel experiments. Observations show that the effect of gravity and the resulting vertical separation of droplets of different sizes are almost negligible under in-cloud icing conditions, where droplets are small and air velocity is relatively higher. However, droplet size increases significantly towards the bottom of the tunnel under freezing drizzle conditions, where droplets are larger and air velocity is relatively lower. The MVD at the height of nozzles is always greater at the end of simulation than at the beginning, which results mainly from the coalescences following droplet collisions. Turbulence dispersion amplifies the effect of droplet collision and causes the occurrence of droplets in a wider vertical domain, whereas the influence of evaporation becomes more significant when air temperature increases or relative humidity of air decreases. Both computed and measured results reveal these tendencies clearly, and satisfactory coincidence was obtained between them even quantitatively. Our former model has been improved successfully, although droplet size is still slightly underestimated in the top half of the tunnel, droplets are dispersed in a wider range, which is in accordance with experimental findings, and the model provides an excellent prediction of droplet sizes measured in the bottom half of the tunnel.

Acknowledgments

This research was carried out within the framework of the NSERC/Hydro-Québec Industrial Chair on Atmospheric Icing of Power Network Equipment (CIGELE) and the Canada Research Chair on Atmospheric Icing Engineering of Power Network (INGIVRE) at the University of Québec at Chicoutimi. The authors would like to thank all the sponsors of the CIGELE for their support. We would also like to thank Z. Péter for his valuable help in CFX computations, and A.R. Karev for his help in measuring the turbulence data.

Appendix

Parameters which are constant throughout the simulation:

c_w	specific heat of water	4.27×10^3 J/(kg K)
L_{ev}	latent heat of water vaporization	2.5×10^6 J/kg
M_a	molecular mass of air	28.964 g/mol
M_w	molecular mass of water	18.016 g/mol
p_{st}	static pressure of air	101325 Pa
Pr	Prandtl number	0.72
R	universal gas constant	8.3144 J/(mol K)
R_w	gas constant for water vapour	R/M_w
Sc	Schmidt number	0.63
ρ_d	density of water droplet	1000 kg/m^3

Parameters calculated as functions of temperature (Pruppacher and Klett, 1978):

D_w	diffusion coefficient of water vapor	$2.11 \times 10^{-5}(T_a/273.16)^{1.94}$	T_a (K)
e_w	pressure of saturated water vapor	$6.1368 \times 10^{-9}T_a^6 + 2.0341 \times 10^{-6}T_a^5 + 3.0312 \times 10^{-4}T_a^4 + 2.6506 \times 10^{-2}T_a^3 + 1.4289T_a^2 + 4.4365 \times 10^{1}T_a + 6.1078 \times 10^{2}$	T_a (°C)
Re_a	Reynolds number based on air velocity	$d\lvert\mathbf{u}\rvert\rho_a/\mu_a$	
λ_a	thermal conductivity of air	$2.384 \times 10^{-2} + 7.123 \times 10^{-5}T_a$	T_a (°C)
μ_a	dynamic viscosity of air	$(1.718 + 4.9 \times 10^{-3}T_a - 1.2 \times 10^{-5}T_a^2) \times 10^{-5}$	T_a (°C)
ρ_a	density of air	$p_{st}M_a/(RT_a)$	T_a (K)

The parameters D_w, e_w and μ_a at droplet temperature are calculated using the corresponding formulae given above obtained after replacing T_a by T_d.

References

Ashgriz, N., Poo, J.Y., 1990. Coalescence and separation in binary collisions of liquid drops. J. Fluid Mech. 221, 183–204.

Beard, K.V., Pruppacher, H.R., 1971. A wind tunnel investigation of the rate of evaporation of small water drops falling at terminal velocity in air. J. Atmos. Sci. 28, 1455–1464.

Brazier-Smith, P.R., Jennings, S.G., Latham, J., 1972. The interaction of falling water droplets: coalescence. Proc. Roy. Soc. Lond. A 326, 393–408.

Crowe, C.T., Sharma, M.P., Stock, D.E., 1977. The particle-source-in cell (PSI-CELL) model for gas-droplet flows. J. Fluids Eng., 325–332.

Du, N.D., 1987. Études des méthodes par impact et à l'huile utilisées pour déterminer le diamètre des gouttelettes dans les brouillards naturels et artificiels. M.Sc. thesis, University of Québec at Chicoutimi, Chicoutimi, QC, Canada.

Dukowicz, J.K., 1980. A particle-fluid numerical model for liquid sprays. J. Comput. Phys. 35, 229–253.

Edson, J.B., Anquetin, S., Mestayer, P.G., Sini, J.F., 1996. Spray droplet modeling 2. An interactive Eulerian–Lagrangian model of evaporating spray droplets. J. Geophys. Res. 101, 1279–1293.

Estrade, J.P., Carentz, H., Lavergne, G., Biscos, Y., 1999. Experimental investigation of dynamic binary collision of ethanol droplets – a model for droplet coalescence and bouncing. Int. J. Heat Fluid Flow 20, 486–491.

Gates, E.M., Lam, W., Lozowski, E.P., 1988. Spray evolution in icing wind tunnels. Cold Reg. Sci. Technol. 15, 65–74.

Gavaises, M., Theodorakakos, A., Bergeles, G., Brenn, G., 1996. Evaluation of the effect of droplet collisions on spray mixing. Proc. Inst. Mech. Eng. 210, 465–475.

Godard, S., 1960. Mesure de gouttelettes de nuage avec un film de collargol. Bull. de l'Observatoire du Puy de Dome, 41–46.

Gore, R.A., Crowe, C.T., 1989. Effect of particle size on modulating turbulent intensity. Int. J. Multiphase Flow 15, 279–285.

Gosman, A.D., Ioannides, E., 1981. Aspects of computer simulation of liquid-fuelled combustors. AIAA Paper 81-023.

Hetsroni, G., 1989. Particles–turbulence interaction. Int. J. Multiphase Flow 15, 735–746.

Ko, G.H., Ryou, H.S., 2005. Droplet collision processes in an inter-spray impingement system. J. Aeros. Sci. 36, 1300–1321.

Kollár, L.E., Farzaneh, M., Karev, A.R., 2005a. Modeling droplet collision and coalescence in an icing wind tunnel and the influence of these processes on droplet size distribution. Int. J. Multiphase Flow 31, 69–92.

Kollár, L.E., Farzaneh, M., Karev, A.R., 2005b. The role of droplet collision, evaporation and gravitational settling in the modeling of two-phase flows under icing conditions. in: Proc. of the 11th International Workshop on Atmospheric Icing of Structures, Montreal, QC, Canada, Paper IW38.

Kollár, L.E., Farzaneh, M., Karev, A.R., 2006. Modeling droplet size distribution near a nozzle outlet in an icing wind tunnel. Atomiz. Sprays 16, 673–686.

Laforte, J.L., Du, N.D., 1988. Comparison of three slide impact methods for measuring the size of water droplets. in: Proc. of the 4th International Workshop on Atmospheric Icing of Structures, Paris, France, pp. 263–267.

Marek, J., Olsen Jr., W.A., 1986. Turbulent dispersion of the icing cloud from spray nozzles used in icing tunnels. in: Proceedings of the 3rd International Workshop on Atmospheric Icing of Structures, Vancouver, BC, Canada, pp. 103–110.

Maxey, M.R., Riley, J.J., 1983. Equation of motion for a small rigid sphere in a nonuniform flow. Phys. Fluids 26, 883–889.

Orme, M., 1997. Experiments on droplet collisions, bounce, coalescence and disruption. Prog. Energy Combust. Sci. 23, 65–79.

O'Rourke, P., Bracco, F., 1980. Modeling of drop interactions in thick sprays and a comparison with experiments. Proc. Inst. Mech. Eng. 9, 101–116.

Post, S.L., Abraham, J., 2002. Modeling the outcome of drop–drop collisions in Diesel sprays. Int. J. Multiphase Flow 28, 997–1019.

Pruppacher, H.R., Klett, J.D., 1978. Microphysics of Clouds and Precipitation. D. Reidel Publishing Company, Dordrecht, Holland.

Qian, J., Law, C.K., 1997. Regimes of coalescence and separation in droplet collision. J. Fluid Mech. 331, 59–80.

Snyder, W.H., Lumley, J.L., 1971. Some measurements of particle velocity autocorrelation functions in a turbulent flow. J. Fluid Mech. 48, 41–71.

Valentine, J.R., Decker, R.A., 1995. A Lagrangian–Eulerian scheme for flow around an airfoil in rain. Int. J. Multiphase Flow 21, 639–648.

Wang, L.-P., Ayala, O., Kasprzak, S.E., 2005. Theoretical formulation of collision rate and collision efficiency of hydrodynamically interacting cloud droplets in turbulent atmosphere. J. Atmos. Sci. 62, 2433–2450.

Whitaker, S., 1972. Forced convection heat transfer correlations for flow in pipes, past flat plates, single cylinders, and for flow in packed beds and tube bundles. AIChE J. 18, 361–371.